Structure-based design of selective and potent G quadruplex-mediated telomerase inhibitors

Martin Read*†, R. John Harrison*†, Barbara Romagnoli*, Farial A. Tanious‡, Sharon H. Gowan§, Anthony P. Reszka*, W. David Wilson‡, Lloyd R. Kelland§, and Stephen Neidle*¶

*Cancer Research Campaign Biomolecular Structure Unit, Chester Beatty Laboratories, The Institute of Cancer Research, London SW3 6JB, United Kingdom; §Cancer Research Campaign Centre for Cancer Therapeutics, The Institute of Cancer Research, Sutton, Surrey SM2 5NG, United Kingdom; and ‡Department of Chemistry and Center for Biotechnology and Drug Design, Georgia State University, Atlanta, GA 30303-3083

Edited by Peter B. Dervan, California Institute of Technology, Pasadena, CA, and approved February 13, 2001 (received for review November 27, 2000)

The telomerase enzyme is a potential therapeutic target in many human cancers. A series of potent inhibitors has been designed by computer modeling, which exploit the unique structural features of quadruplex DNA. These 3,6,9-trisubstituted acridine inhibitors are predicted to interact selectively with the human DNA quadruplex structure, as a means of specifically inhibiting the action of human telomerase in extending the length of single-stranded telomeric DNA. The anilino substituent at the 9-position of the acridine chromophore is predicted to lie in a third groove of the quadruplex. Calculated relative binding energies predict enhanced selectivity compared with earlier 3,6-disubstituted compounds, as a result of this substituent. The ranking order of energies is in accord with equilibrium binding constants for quadruplex measured by surface plasmon resonance techniques, which also show reduced duplex binding compared with the disubstituted compounds. The 3,6,9-trisubstututed acridines have potent *in vitro* inhibitory activity against human telomerase, with EC_{50} values of up to 60 nM.

The telomeric ends of chromosomes consist of tandem repeats of simple guanine-rich DNA protein-associated motifs whose function is to protect the ends from unwanted DNA damage-repair, recombination, and end-fusions. In eukaryotics the repeat is TTAGGG, with telomere length varying between *ca.* 5 and 15 kb (1, 2). Cancer cells typically have short telomeres, whereas stem cell telomere length tends to be at the high end of this range. The terminal 150–200 bases at the 3′ end of human telomeres form a single-stranded overhang, whose exact structure is not fully established, although loop-type arrangements have been suggested from electron microscope studies (3). Telomeres shorten in somatic cells on each round of replication, by 50–200 bases, as a consequence of the inability of DNA polymerase to fully replicate the ends (4). Once telomeres reach a critically short length, cells enter a senescent state and do not replicate further (5). By contrast, the short telomeres in tumor cells are stable in length, maintained by the action of a specialized DNA polymerase, the telomerase enzyme complex, which catalyses the synthesis of further telomere repeats (6). Telomerase is activated in 80–90% of human tumors and is undetectable in most normal somatic cells (7). This activation has been shown to be a key step in the immortalization process in human cells, leading to tumorigenesis (8). A small proportion of tumor cells have an alternative telomere maintenance pathway (ALT) which appears to be independent of telomerase and involves recombination events. Inhibition of telomerase by a dominant negative mutant (9, 10), or by synthetic oligonucleotides targeted to the RNA template (11), leads to telomere shortening, growth arrest and apoptosis for tumor cells in culture. Telomerase is thus a highly attractive target for selective anti-cancer therapy (12).

We have focused on the rational discovery of small-molecule telomerase inhibitors with pharmacologically acceptable features, and which are predicted to interact with the DNA telomere primer strand rather than the enzyme itself. Telomerase requires the 3′ end of the primer to be single-stranded to effectively hybridize with the enzyme's endogenous RNA template, and possibly for effective precession of the newly synthesized strand to occur. Folding of telomeric DNA into four-stranded guanine-quadruplex (G4) structures (13) has been shown to inhibit the enzyme from catalyzing the synthesis of further telomeric DNA repeats (14). Synthetic molecules that stabilize such G4 structures may then be effective telomerase inhibitors (15). A number of G4 inhibitors have been identified, based on the tricyclic aromatic chromophores anthraquinones (16, 17), fluorenones (18), and acridines (19, 20), as well as a perylenetetracarboxylic diimide derivative (21) and compounds with a porphyrin skeleton (22). For the majority of these molecules optimal activity has been achieved by substitution of side chains possessing amidoalkylamino character. The best of these ligands have telomerase activity of *ca.* 2–5 μM, expressed as the concentration to inhibit 50% of enzymatic telomere-lengthening function; acute cytotoxicities as measured by 96-h exposures in ovarian tumor cell lines are also typically at this level (16–20).

The classic model for telomere maintenance by telomerase suggests that inhibitors will require administration for a considerable number of rounds of cell doubling for sufficient telomere attrition to occur so that senescence is triggered. The requisite concentration of inhibitor needs to be significantly below acute toxicity levels, otherwise generalized cytotoxic cell kill will take place instead. Conventional antitumor agents that bind to duplex DNA typically produce their cytotoxic effect by interfering with transcription or with the correct function of DNA topoisomerases or other enzymes involved in DNA replication. The G4 inhibitors reported to date generally have affinity for duplex DNA comparable to their quadruplex binding, and it is unsurprising that levels of cytotoxicity and telomerase inhibition also have been found to be comparable (see above). Modest duplex vs. quadruplex selectivity has been reported for some substituted porphyrins (23). The hypothesis that telomerase inhibition occurs via a quadruplex-mediated mechanism would be strongly supported by a molecule that shows (*i*) G4 selectivity over duplex DNA affinity, and (*ii*) increased potency for telomerase inhibition, together with a low level of acute cytotoxic activity.

G4 DNAs have several distinct structural features compared with duplex DNA (13), notably the possession of four quasi-equivalent grooves and a pronounced channel of negative electrostatic potential running through the center of the planes of G quartets, allowing metal ions to be coordinated between the planes in a bipyramidal antiprismatic manner. We report here the rational design and evaluation of a series of molecules that take account of these features and that have enabled significant G4 selectivity to be achieved. They are derived in part from our earlier studies (16–20), which have resulted in compounds

This paper was submitted directly (Track II) to the PNAS office.

Abbreviations: SPR, surface plasmon resonance; TRAP, telomeric repeat amplification protocol.

†M.R. and R.J.H. contributed equally to this work.

¶To whom communications should be addressed. E-mail: s.neidle@icr.ac.uk.

The publication costs of this article were defrayed in part by page charge payment. This article must therefore be hereby marked "*advertisement*" in accordance with 18 U.S.C. §1734 solely to indicate this fact.

 www.pnas.org/cgi/doi/10.1073/pnas.081560598

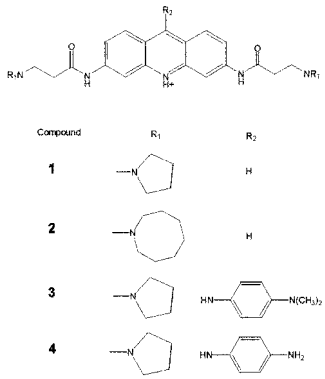

Fig. 1. Structures of compounds **1**–**4**.

typified by the disubstituted acridine (**1**: Fig. 1). These showed that simulating the energetics and geometry of ligand binding to the structure of the human intramolecular G quadruplex formed by the 22-mer d[$AG_3(TTAG_3)_3$] provided good correlations with their telomerase inhibition. This NMR-derived G4 structure (24) has been used as a starting point for the present molecular design studies, focusing on a single high-affinity binding site stacked on one end of the plane of G quartets in the structure (25).

Materials and Methods

Molecular Modeling. The coordinates from one of the solution NMR structures of the folded intramolecular G-quadruplex human telomeric repeat d[$AG_3(TTAG_3)_3$] (Protein Data Bank entry 143D) were taken as a starting model. It was initially subjected to molecular mechanics energy minimization (1,000 steps steepest descent and 3 × 1,000 steps Polak-Ribiere conjugate gradient), followed by 140 ps of molecular dynamics simulation (1.5-fs time step at 300 K). The subsequent time-averaged structure was further minimized (1,000 steps steepest descent and 3 × 1,000 steps Polak-Ribiere conjugate gradient) and used as the basis for all further modeling studies. The AMBER 6.0 suite of molecular simulation programs (26) and the Cornell *et al.* force field (27) were used in these and subsequent computations.

A pseudointercalation ligand binding site was introduced between the diagonal T_2A loop and the G-quartet segment of the structure (at the 5′ AG step) by breaking the two phosphate backbones and separating the two halves of the structure so that the separation of the A:A base pair and G quartet increased from 3.4 to 6.8 Å. The sugar-phosphate chains were reconnected, and molecular mechanics energy minimization (1,000 steps steepest descent followed by 1,000 steps conjugate gradient) was used to relieve any resulting steric distortion while retaining the intercalation geometry between G quartet and loop motifs by means of appropriate positional restraints.

A molecular models of the acridine derivative **1** was built and charges were allocated by using the AM1 semiempirical formalism in the MOPAC package (28). The ligand then was minimized and manually docked into the pseudointercalation site. Ligand positions and orientations also were optimized with the AFFINITY docking program, within the INSIGHT II suite (29). This program incorporates manual and automatic docking procedures and allows nonbonded van der Waals and electrostatic interactions to be monitored during the docking so that many possible conformations can be interactively evaluated. A search also was made for other high-affinity ligand binding sites on the quadruplex; none were found of equivalent binding energy. Flexible ligand docking also was used to define the lowest energy position for the ligand by using a Monte Carlo automated docking protocol. The G quartets were restrained to their original positions throughout the docking protocols. The final low energy conformation of the ligand then was subjected to a further 500 steps of unrestrained molecular mechanics minimization before it was transferred to the AMBER 6.0 suite. The force-field parameters for the ligand were extrapolated from existing values for analogous groups in the AMBER and CFF force fields (29). Visual inspection together with chemical insight was used to conceptualize derivatives of compound **1**, which would produce increased van der Waals contacts with the binding site. Compounds **3** and **4** were designed in this way. Molecular dynamics simulation computations on them and their complexes were performed with protocols identical to those for compound **1**.

DNA-ligand complexes were solvated in a periodic TIP3 water box of dimensions ≈60 × 60 × 60 Å, which extended at least 10 Å from any solute atom. Two internal sodium ions were positioned in the central channel between the three central G quartets by using crystallographically determined distances from the d(TG_4T) crystal structure (13). The sodium ions were positioned to allow coordination with the four polarized carbonyl oxygens on the two adjacent G quartets, completing the octahedral coordination sphere. Each system then required an additional 18 sodium counter ions for complete neutralization. These were positioned throughout the cell at grid points of negative coulombic potential.

All calculations were carried out by using the Sander module of AMBER 6.0 with the SHAKE algorithm enabled for the hydrogen atoms and a 2-fs time step. The nonbonded pairs list was updated every 20 steps. Each complex was subjected to 1,000 steps of conjugate gradient minimization followed by 10 ps of equilibration dynamics at 300 K with full constraints on the DNA complex and a 12-Å nonbonded Lennard-Jones cutoff. The particle mesh Ewald summation term was activated for all simulations to include long-range electrostatic interactions in the calculations. The particle mesh Ewald charge grid spacing was ≈1.0 Å, and the charge grid was chosen to be products of the powers of two, three, and five to ensure efficiency of the fast Fourier transform calculation. Each complex then was gradually allowed to relax as restraints were sequentially lowered over seven successive rounds of conjugate gradient minimizations. For dynamics runs after minimizations, the initial velocities were assigned by using the standard Maxwellian distributions. The final production run of 1,000 ps was then carried out on a multiple-processor SGI Origin 200 computer. Coordinates were written to the output files every 5 ps for the analysis of the trajectory. Relative binding energies for all three compounds were calculated by subtracting the total interaction energy of the explicitly solvated ligand and its surroundings in a neutral periodic box from the identical system, when the ligand was bound to the folded human G4 DNA structure. The resulting differences in interaction energy correspond to relative binding energies. These procedures did not produce meaningful binding energies for compound **2**. Attempts at simulating its binding resulted in distortions to the quadruplex structure such that the ligand was shifted by 2.5–4 Å from the bound positions of the other compounds, as a result of the bulky side chains.

Preparation of 3,6,9-Trisubstituted Acridine Derivatives. Compounds **3** and 4 were synthesized by the routes shown in Fig. 2, via acridone intermediates. Full details will be given elsewhere. In both cases the final substitution step gave product in 88% yield. Both compounds were analytically pure. Compounds **1** and **2** were synthesized as described (19).

Binding and Kinetic Studies. Surface plasmon resonance (SPR)measurements were performed by using a BIACore 2000 system with streptavidin-coated sensor chips (SA) for all experiments. This chip consists of a gold surface and streptavidin covalently immobilized on a carboxymethylated dextran layer at the surface. To prepare sensor chips for use, they were conditioned with three consecutive 1-min injections of 1 M NaCl in 50 mM NaOH followed by extensive washing with buffer. Biotinylated DNA (5′-Biot-d[$AG_3(TTAG_3)_3$]) in Hepes buffer, pH 7.4 [0.01 M Hepes, 0.15 M NaCl, 3 mM EDTA,

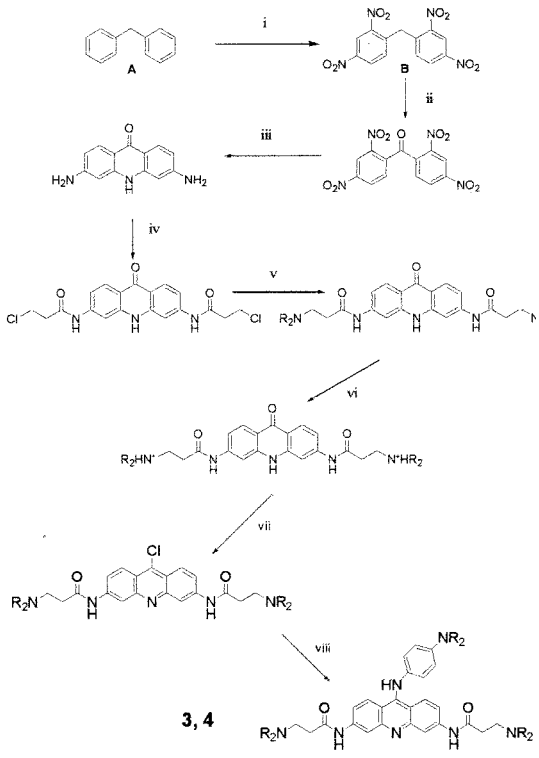

Fig. 2. Synthetic schemes for the 3,6,9-trisubstituted acridine derivatives **3** and **4**. The individual steps involved (*i*) KNO_3/H_2SO_4, (*ii*) CrO_3, AcOH, reflux, (*iii*) Zn/HCl, 90–100°C, (*iv*) 3-CPC, reflux, (*v*) NHR_2, EtOH, NaI, reflux, (*vi*) HCl, (*vii*) $POCl_3$, reflux, and (*viii*) H_2NPhNR_2, $CHCl_3$, rt.

and 0.005% (vol/vol) Surfactant P20] was immobilized on the surface by noncovalent capture to streptavidin. One of the flow cells was used to immobilize the DNA and another served as a control. Manual injection was used with 25 nM DNA and a flow rate of 2 μl/min to achieve long contact times with the surface and to control the amount of the DNA bound to the surface. This DNA folded in the presence of K^+ and formed a quadruplex during extended flow in the SPR experiments. (Folding with respect to time was checked by a series of melting/cooling experiments assessed by both CD and UV methods; after several minutes of cooling to 25°C, no further change in signals with respect to time was observed.) A second channel of the sensor chip was left as a blank reference. All procedures for binding studies were automated by using repetitive cycles of sample injection and regeneration.

All ligand samples were dissolved in H_2O (1 mM) and then diluted as stock solution to 1E-4M in the running buffer, pH 7.4 (0.01 M Hepes/0.2 M KCl/3 mM EDTA/50 μl/liter Surfactant P20). Samples of each were prepared in filtered and degassed buffer by serial dilutions from the stock solutions. The same running buffer was used for regeneration of the surface.

Samples were injected at flow rates of 10–20 μl/min by using the KINJECT command for steady-state experiments. A higher flow rate of 100 μl/min was used for the kinetic experiments to minimize mass transport effects and deliver a consistent sample plug. Double referencing subtractions were used for data analysis. The first reference subtraction eliminates the bulk refractive index change and injection noise whereas the second subtraction of a blank buffer injection eliminates any systematic changes that are characteristic of a particular cell. Details of the data analysis will be given elsewhere.

***Taq* Polymerase Assay.** Ligands were evaluated as their acid addition hydrochloride salts at 10, 20, and 50 μM final concentrations in a PCR 50 μl master mix containing 10 ng pCI-neo mammalian expression vector (Promega) and forward d(GGAGTTCCGCGTTACATAAC) and reverse d(GTCTGCTCGAAGCATTAACC) primers (200 nmol) as described (17). The product of ≈1 kb was visualized on a 2% (wt/wt) agarose gel after amplification (30 cycles of 94°C for 1 min, 55°C for 1 min, and 72°C for 2.5 min).

Modified Telomeric Repeat Amplification Protocol (TRAP) Assay. The ability of compounds **1–4** to inhibit telomerase in a cell-free assay was assessed with a modified TRAP assay using extracts from exponentially growing A2780 human ovarian carcinoma cells as described (17–19). The TRAP assay was performed in two steps: (*i*) telomerase-mediated extension of the forward primer (TS: 5′-d(AATCCGTCGAGCAGAGTT), Oswel, Southampton, U.K.) contained in a 40 μl reaction mix comprising TRAP buffer [20 mM Tris·HCl (pH 8.3)/68 mM KCl/1.5 mM $MgCl_2$/1 mM EGTA/0.05% (vol/vol) Tween 20/0.05 μg BSA/50 μM of each deoxynucleotide triphosphate/0.1 μg TS primer/3 μCi of [α-^{32}P]dCTP (Amersham Pharmacia)]. Protein (0.04 μg) then was incubated with the reaction mix ± agent (as acid addition salts) at final concentrations of up to 50 μM for 20 min at 25°C. A lysis buffer (no protein) control, heat-inactivated protein control, and 50% protein (0.02 μg) control were included in each assay. (*ii*) While heating at 80°C in a PCR block of a thermal cycler (Hybaid, Middlesex, U.K.) for 5 min to inactivate telomerase activity, 0.1 μg of reverse CX primer [3′-d(AATCCCATTCCCATTCCCATTCCC-5′)] and 2 units of *Taq* DNA polymerase ("red hot", Advanced Biotechnologies, Columbia, MD) were added. A three-step PCR was then performed: 94°C for 30 s, 50°C for 30 s, and 72°C for 1 min for 31 cycles. Telomerase-extended PCR products in the presence or absence of the ligands then were determined either by electrophoretic separation using 8% (wt/wt) acrylamide denaturing gels and analysis by phosphorimaging or autoradiography, or by harvesting on Whatman filters (25-mm glass microfiber) and analysis by liquid scintillation counting.

Growth Inhibition Assay. Growth inhibition was measured in three telomerase-positive human ovarian carcinoma cell lines (A2780, CH1, and SKOV-3) using the sulforhodamine B assay as described (17–19). Briefly, between 3,000 and 6,000 cells were seeded into the wells of 96-well microtiter plates and allowed to attach overnight. Agents (acid addition and quaternary dimethiodide salts) were dissolved at 500 μM in water and immediately added to wells in quadruplicate at final concentrations of 0.05, 0.25, 1, 5, and 25 μM. After an incubation period of 96 h, remaining cells were fixed with ice-cold 10% (wt/vol) trichloroacetic acid (30 min) and stained with 0.4% sulforhodamine B in 1% (vol/vol) acetic acid (15 min). Mean absorbance at 540 nm for each drug concentration was expressed as a percentage of the control untreated well absorbance, and IC_{50} values (concentration required to inhibit cell growth by 50%) were determined for each agent.

Results

Molecular Modeling and Synthesis of Quadruplex-Selective Inhibitors. The initial docking and subsequent dynamics simulations modeling studies show that the planar chromophore of the di-substituted acridine derivative **1** is stacked on the terminal G quartet in the 5′ AG step site, between the 5′ T_2A loop and a terminal G-quartet such that the cationic acridine ring nitrogen atom is overlapping the central polarized carbonyl channel of negative electrostatic potential that runs through the stack of G quartets (Fig. 3*a*). The chromophore is stabilised by π-π stacking interactions with the terminal G quartet and the A:A base pair. The binding site itself is highly asymmetric, and because it is external to the stack of three G quartets, it is bounded by the grooves formed by the phosphodiester backbones. The two substituent amidoalkylamino chains lie in the two widest grooves, with the terminal pyrrolidine rings forming favorable hydrophobic interactions with the sides of the grooves. A

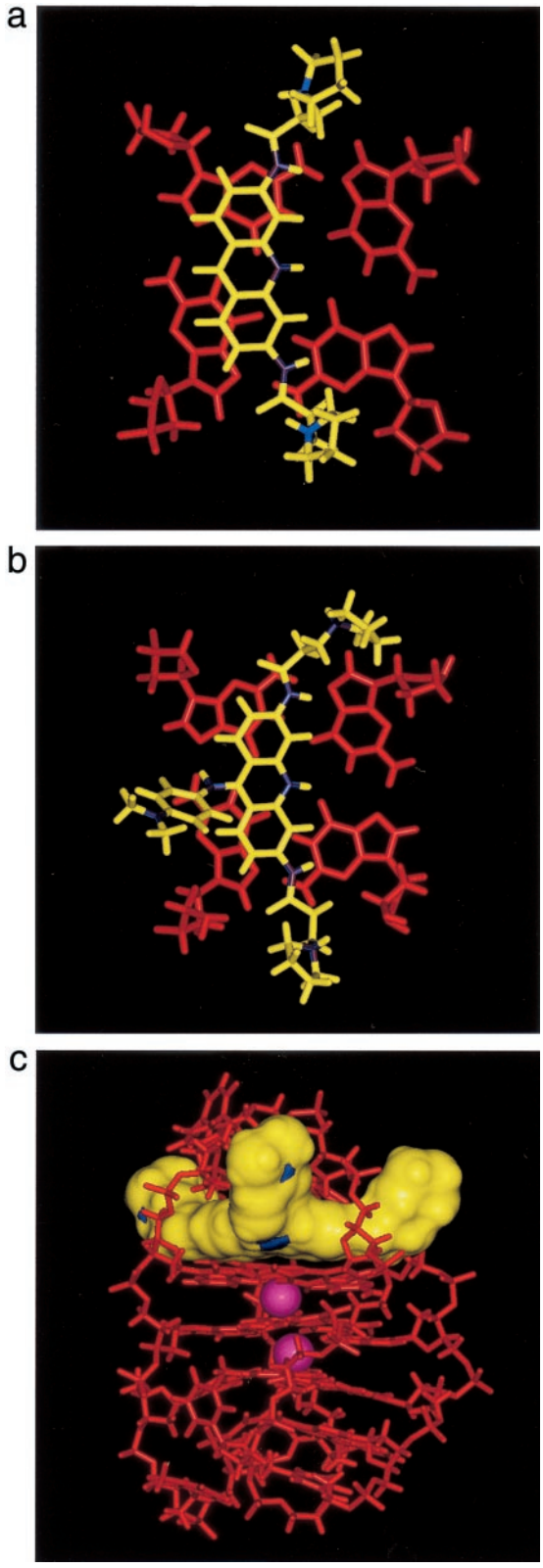

Fig. 3. (*a*) View of the simulated structure of compound **1** bound to the high-affinity binding site in the human quadruplex structure formed from the sequence d[$AG_3(TTAG_3)_3$], looking onto the terminal guanine quartet. (*b*) View of the complex with compound **3** bound in the same site, at the end of a 1-ns molecular dynamics simulation. (*c*) Overall view of the complex with compound **3** (shown as a solvent-accessible surface, with nitrogen atoms highlighted in blue). The two sodium atoms in the central channel of the G quartet are shown in mauve.

third groove, between the extreme 5′ end of the sequence and residues 13–15, has a narrowed width of <6 Å.

Initial molecular modeling studies on further compounds, with aliphatic substituents at the 9-position, indicated that these would sit directly in the third groove, resulting in an increased interaction energy. These models suggested that the ideal chain length was only *ca.* 4–5 carbon atoms to maximize the van der Waals interactions in the third groove, by contrast with the longer amidoalkylamino side chains. This shorter distance is brought about by the slightly closer position of the acridine chromophore to the third groove. Hence, any substituent at this position could potentially introduce steric clashes with the adjacent G quartet interfering with the essential 3.4-Å stacking interactions. Models of these systems indicated that direct attachment of an aliphatic carbon linker to the chromophore would indeed produce such steric clashes. The original side chains in **1** and other compounds incorporate an amide functionality that conjugates with the ring system and maintains planarity to the edge of the G quartet, thus eliminating any potential steric clashes. By analogy we have found that an amine at the 9-position is not only a synthetically accessible linker, but crucially can be readily accommodated in the binding site without steric hindrance. An aryl substituent attached to the amine would then effectively occupy the space in the third groove.

The first two compounds, **3** and **4**, in this generation of acridine molecules are shown in Fig. 1, having anilino subsituents at the 9-position. Retention of the acridine chromophore ensures that electrostatic interactions are maximized with the top of the central G quartet channel, which has a region of negative electrostatic potential arising from the O6 oxygen atoms of the guanines. The calculated relative binding energies for these compounds are shown in Table 1 and clearly indicate that substitution at the 9-position on the acridine chromophore significantly increases the interaction energy between the ligand and the intramolecular human quadruplex structure. Fig. 3 *b* and *c* shows the final position of compound **3** after 1 ns of unrestrained molecular dynamics. All of the side chains reside in their respective separate grooves without significant conformational changes in the drug molecule. The solvent accessible surface area is shown in Fig. 3*c*, where the drug molecule in yellow complements the surface area of the binding site. Over the trajectory the narrow groove containing the anilino moiety expands to accommodate the aromatic ring, so that all of the grooves become almost identical in width. The slight difference in binding energy between the dimethyl anilino derivative (compound **3**) and the free amine derivative (compound **4**) can be attributed to the protrusion of the *N*-dimethyl moiety into bulk solvent, which thus loses interaction energy with the groove compared with the NH_2 group in **4**. Modeling (detailed elsewhere) also indicated that a B-form DNA duplex, with just two grooves, could only accommodate these tri-substituted molecules with substantial distortion to avoid steric clashes with backbones.

On the other hand, we find that compound **2** is unable to bind effectively, as described (20), due to the large size of the groups at the end of the two side chains, preventing them from forming these favorable contacts.

Interactions with Quadruplexes in Solution. The binding of all four ligands to the human quadruplex and a representative duplex structure was examined by SPR techniques, with the DNA sequences immobilized on chips (Fig. 4). This has provided quantitative estimates of binding affinities and on/off rates of reaction.

The SPR data for all four compounds shows in each case a single strong quadruplex binding site, although weaker ones are also present. The data in Tables 2 and 3 shows that there are marked differences in their affinities for different DNA structures, especially when compared with their binding to duplex DNA. The disubstituted compound **1** has approximately the same binding constant for duplex and quadruplex, whereas the two trisubstituted compounds **3** and **4** bind to human quadruplex

Table 1. Computed interaction energies for the complexes of the three acridine derivatives with the human intramolecular quadruplex, in kcal mole^{-1}

Acridine derivative	Average interaction energy DNA-ligand complex	Average interaction energy for ligand	Relative DNA-ligand binding energy
1	−157.3	−96.3	−61.0
3	−223.6	−132.9	−90.7
4	−220.5	−115.3	−105.2

DNA 30–40 times more strongly than to duplex. Their affinity for the quadruplex is 10-fold higher than that of compound **1**. Compound **2** is the weakest duplex and quadruplex binder of the series.

The kinetics of interactions between the four acridine compounds and the human telomeric DNA G quadruplex also were examined by SPR experiments. High flow rates were used to minimize the effects of mass transport and deliver a consistent sample plug. To collect kinetic data, a range of concentrations of the acridine were injected over the immobilized DNA and reference surface. Responses from the reference surface were used to correct for refractive index changes and instrument noise. A detailed kinetic analysis was performed by globally fitting the association and dissociation phase data for each compound binding to the G quadruplex (Fig. 4*a*). The rate constants are shown in Table 2. The association rate for compound **1** was approximately twice as fast as that for **4** and more than five times that for **3**. Compound **2** was the slowest. The dissociation rate for **1** was approximately 1 order of magnitude faster than that for **4** and 20 times that for **3**. Together these rate constants predict equilibrium association constants for compounds **3** and **4** binding to quadruplexes, which are an order of magnitude higher than that for **1**.

We conclude that the trisubstituted compounds demonstrate significant quadruplex selectivity both in thermodynamic and kinetic terms.

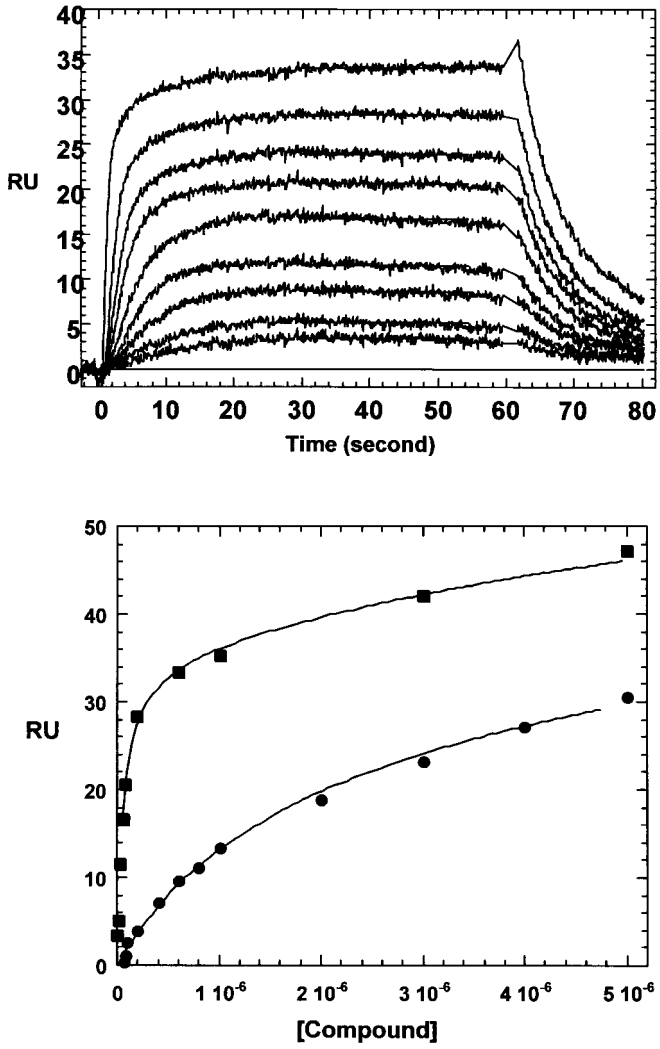

Fig. 4. (*a*) A set of SPR sensorgrams for binding of compound **3** to the human G quadruplex at 25°C is shown. The unbound ligand concentrations in the flow solution were 0, 5, 10, 20, 40, 60, 80, 100, 200, and 600 nM from the lowest curve to the top curve. The lines are linear best fits to the steady-state RU (response units) values, which are directly proportional to the amount of bound compound, and were used to determine the RU for each free ligand concentration. (*b*) The RU values from the steady-state region from *a* plotted versus the unbound compound **3** (■) concentration. Experiments similar to those in *a* also were conducted for compound **1** (●) and curves for the two derivatives are shown. The lines were obtained by nonlinear least-square fits of the data. Results for compound **4** were similar to those for **3**. Equilibrium constants for all compounds are given in Table 3.

Telomerase Inhibition and Cytotoxicity. The TRAP assay used to assess telomerase activity uses PCR amplification of the telomere primer strand. To eliminate false positives in this assay, we used an initial screen with TAQ polymerase, which also helps to identify nonspecific polymerase activity. None of the three compounds in this study were active against TAQ polymerase at concentrations <20 μM. Table 4 summarizes telomerase inhibitory activity and cytotoxicity in three human ovarian carcinoma cell lines, expressed as IC_{50} values, i.e., the concentrations required to inhibit activity and cell growth respectively by 50%. The activity of the disubstituted acridine **1** is typical of the more active anthraquinones, acridines, and other G-quadruplex inhibitors previously reported (16–19). Compound **2** is essentially inactive as a telomerase inhibitor, although it retains the high cytotoxicity of compound **1**. The two trisubstituted compounds **3** and **4**, on the other hand, show telomerase activity at levels of up to *ca.* 100-fold greater potency. Both are also significantly less potent in the cytotoxicity assay, with compound **4** having outstandingly low activity (as well as being the most potent telomerase inhibitor).

Conclusions

There are several lines of evidence supporting the hypothesis of G-quadruplex mediation in the inhibition of telomere elongation by ligands. For example, primer extension results with disubstituted amidoanthraquinones are consistent with the formation of a 3–4 repeat intramolecular quadruplex (16). Structure-activity studies with a series of acridines and anthraquinones disubstituted with

Table 2. Rate constants for quadruplex interactions, determined from BIAcore analysis

Compound	k_a ($M^{-1}\cdot s^{-1}$)	k_d (s^{-1})
1	1.3×10^6	0.272
2	4.6×10^4	0.090
3	2.4×10^5	0.018
4	6.6×10^5	0.029

Table 3. Equilibrium binding constants to duplex and quadruplex DNA

Compound	K (duplex)	K (quadruplex)
1	1.1×10^6	1.3×10^6
2	2×10^5	8.3×10^5
3	4×10^5	1.6×10^7
4	5×10^5	1.6×10^7

Table 4. Telomerase inhibition, and cytotoxicity, given as EC_{50} and IC_{50} values in μM

Compound	$^{tel}EC_{50}$	A2780 IC_{50}	CH1 IC_{50}	SKOV-3 IC_{50}
1	5.2	2.65	8.2	2.6
2	>50	1.3	2.2	2.3
3	0.095	10	10.1	13
4	0.06	>25	>25	>25

progressively increasingly bulky substituents have demonstrated a close relationship between telomerase inhibition and predicted binding energy for the human quadruplex (20). The present study confirms and extends these conclusions, with the successful design of ligands that couple enhanced quadruplex affinity with increased telomerase potency. On the other hand, compound **2**, with increased steric bulk such that it cannot as effectively interact with the quadruplex binding site, is a poor telomerase inhibitor. The improvement in telomerase inhibitory activity shown by the trisubstituted acridines compared with disubstituted one, is qualitatively what would be expected on the basis of their differences in quadruplex affinity alone. It also suggests that further improvements in both quadruplex selectivity/affinity and telomerase activity may be expected upon the incorporation of further appropriate functionality to these and other ligands. Fine-tuning of ligand design and crystallographic studies (if feasible) also may enable one to differentiate between different types of inter and intramolecular quadruplexes that can in principle be formed.

The present results also provide further support for models with ligand bound on the exterior of the stack of G quartets in a quadruplex (21, 25). Alternative models, in which a ligand is intercalated within the stack, are not in accord with NMR evidence (21) or detailed molecular dynamics studies (25). Unwinding and opening up of a G quartet stack (and disruption of the metal-ion structure) would be expected to be exceptionally slow, and is not consistent with the kinetic data in Table 2. Future crystallographic studies will undoubtedly resolve this issue.

The classic model for telomerase activity focuses on its role of catalyzing telomere length extension, with inhibition resulting in telomere shortening and senescence. There is recent evidence of an additional and more complex role for the enzyme, of capping telomere ends and so protecting them from entering DNA damage pathways (30, 31). In this way telomerase maintains the integrity of the very short telomeres characteristic of many tumor cells. A consequence of this model is that interference with the capping function will lead to the activation of DNA damage response and eventual cell death. The folding of telomeric ends into higher-order quadruplex structures is known to inhibit telomerase catalytic activity (14), probably by disallowing the initial template-primer recognition from occurring. Thus the action of quadruplex-selective ligands, such as are described here, is fully consistent with the capping model, and moreover provides an explanation for findings (S.H.G. and L.A.K., unpublished observations) of cellular senescence produced by compounds **3** and **4** in the absence of significant telomere shortening.

Telomerase-negative (ALT) mechanisms of telomere maintenance are likely to involve end-to-end recombination events (33) such as higher-order telomeric DNA formation and disassembly promoted by helicases. One such, the Bloom's syndrome helicase is implicated in the high level of recombination events that characterize this disorder and has also been found to unwind quadruplex DNA (34) more readily than duplex DNA. The perylene quadruplex-interactive ligand (21) has been found (32) to inhibit the unwinding of the analogous helicase from *Saccharomyces cerevisiae*, suggesting that it and other G4 ligands may be effective inhibitors of G4-mediated recombination in general, and perhaps of ALT mechanisms in particular. This would give G4-interactive ligands the therapeutic advantage over other categories of telomerase inhibitors (11, 12), of being active in telomerase-negative ALT cell lines.

1. McEachern, M. J., Krauskopf, A. & Blackburn, E. H. (2000) *Annu. Rev. Genet.* **34,** 331–358.
2. Williamson, J. R. (1994) *Annu. Rev. Biophys. Biomol. Struct.* **23,** 703–730.
3. Griffith, J. D., Comeau, L., Rosenfield, S., Stansel, R. M., Bianchi, A., Moss, H. & de Lange, T. (1999) *Cell* **97,** 503–514.
4. Bryan, T. M. & Cech, T. R. (1999) *Curr. Opin. Cell. Biol.* **11,** 318–324.
5. Harley, C. B., Futcher, A. B. & Greider, C. W. (1990) *Nature (London)* **345,** 458–460.
6. Nugent, C. I., Meyerson, M., Counter, C. M., Eaton, E. N., Ellison, L. W., Steiner, P., Caddle, S. D., Ziaugra, L., Beijersbergen, R. L., Davidoff, M. J., *et al*. (1997) *Cell* **90,** 785–795.
7. Kim, N. W., Piatyszek, M. A., Prowse, K. R., Harley, C. B., West, M. D., Ho, P. L. C., Coviello, G. M., Wright, W. E., Weinrich, R. & Shay, J. W. (1994) *Science* **266,** 2011–2015.
8. Hahn, W. C., Counter, C. M., Lundberg, A. S., Beijersbergen, R. L., Brooks, M. W. & Weinberg, R. A. (1999) *Nature (London)* **400,** 464–468.
9. Hahn, W. C., Stewart, S. A., Brooks, M. W., York, S. G., Eaton, E., Kurachi, A., Beijersbergen, R. L., Knoll, J. H. M., Meyerson, M. & Weinberg, R. A. (1999) *Nat. Med.* **5,** 1164–1170.
10. Zhang, X., Mar, V., Zhou, W., Harrington, L. & Robinson, M. O. (1999) *Genes Dev.* **13,** 2388–2399.
11. Herbert, B. S., Pitts, A. E., Baker, S. I., Hamilton, S. E., Wright, W. E., Shay, J. W. & Corey, D. R. (1999) *Proc. Natl. Acad. Sci. USA* **96,** 14276–14281.
12. Neidle, S. & Kelland, L. R. (1999) *Anti-Cancer Drug Des.* **14,** 341–347.
13. Phillips, K., Dauter, Z., Murchie, A. I. H., Lilley, D. M. J. & Luisi, B. (1997) *J. Mol. Biol.* **273,** 171–182.
14. Zahler, A. M., Williamson, J. R., Cech, T. R. & Prescott, D. M. (1991) *Nature (London)* **350,** 718–720.
15. Mergny, J.-L. & Hélène, C. (1998) *Nat. Med.* **4,** 1366–1367.
16. Sun, D. B., Thompson, B., Cathers, B. E., Salazar, M., Kerwin, S. M., Trent, J. O., Jenkins, T. C., Neidle, S. & Hurley, L. H. (1997) *J. Med. Chem.* **40,** 2113–2116.
17. Neidle, S., Harrison, R. J., Reszka, A. P. & Read, M. A. (2000) *Pharmacol. Ther.* **85,** 133–139.
18. Perry, P. J., Read, M. A., Davies, R. T., Gowan, S. M., Reszka, A. P., Wood, A. A., Kelland, L. R. & Neidle, S. (1999) *J. Med. Chem.* **42,** 2679–2684.
19. Harrison, R. J., Gowan, S. M., Kelland, L. R. & Neidle, S. (1999) *Bioorg. Med. Chem. Lett.* **9,** 2463–2468.
20. Read, M. A., Wood, A. A., Harrison, R. J., Gowan, S. M., Kelland, L. R., Dosanjh, H. S. & Neidle, S. (1999) *J. Med. Chem.* **42,** 4538–4546.
21. Federoff, O. Y., Salazar, M., Han, H., Chemeris, V. V., Kerwin, S. M. & Hurley, L. H. (1998) *Biochemistry* **37,** 12367–12374.
22. Han, F. X., Wheelhouse, R. T. & Hurley, L. H. (1999) *J. Am. Chem. Soc.* **121,** 3561–3570.
23. Arthanari, H., Basu, S., Kawano, T. L. & Bolton, P. H. (1998) *Nucleic Acids Res.* **26,** 3724–3728.
24. Wang, Y. & Patel, D. J. (1993) *Structure (London)* **1,** 263–282.
25. Read, M. A. & Neidle, S. (2000) *Biochemistry* **39,** 13422–13432.
26. Case, D. A., Pearlman, D. A., Caldwell, J. C., Cheatham, T. E., Ross, W. S., Simmerling, C., Darden, T., Merz, K. M., Stanton, R. V., Cheng, A., *et al*. (2000) AMBER (Univ. of California, San Francisco), Version 6.0.
27. Cornell, W. D., Cieplak, P., Bayly, C. I., Gould, I. R., Merz, K., Ferguson, D. M., Spellmeyer, D. C., Fox, T., Cardwell, J. W. & Kollman, P. A. (1995) *J. Am. Chem. Soc.* **117,** 5179–5197.
28. Dewar, M. J. S., Zoebisch, E. G., Healy, E. F. & Stewart, J. J. P. (1985) *J. Am. Chem. Soc.* **107,** 3902–3909.
29. Molecular Simulations (1999) INSIGHT II *Modeling Environment* (Molecular Simulations, San Diego).
30. Zhu, J., Wang, H., Bishop, J. M. & Blackburn, E. H. (1999) *Proc. Natl. Acad. Sci. USA* **96,** 3723–3728.
31. Blackburn, E. H. (2000) *Nature (London)* **408,** 53–56.
32. Han, H., Bennett, R. J. & Hurley, L. H. (2000) *Biochemistry* **39,** 9311–9316.
33. Dunham, M. A., Neumann, A. A., Fasching, C. L. & Reddel, R. R. (2000) *Nat. Genet.* **26,** 447–450.
34. Sun, H., Karow, J. K., Hickson, I. D. & Maizels, N. (1998) *J. Biol. Chem.* **273,** 27587–28792.